Global stability analysis of birhythmicity in a self-sustained oscillator

R. Yamapi,[1,a)] G. Filatrella,[2] and M. A. Aziz-Alaoui[3]
[1]*Department of Physics, Group of Nonlinear Physics and Complex System, Faculty of Science, Fundamental Physics Laboratory, University of Douala, Box 24157, Douala, Cameroon*
[2]*CNR-SPIN Salerno and Dipartimento di Scienze Biologiche ed Ambientali, Università del Sannio, via Port'Arsa 11, I-82100 Benevento, Italy*
[3]*Applied Mathematics Laboratory, University of Le Havre, 25 Rue Ph. Lebon, B.P. 540, Le Havre, Cedex, France*

(Received 29 March 2009; accepted 14 January 2010; published online 9 March 2010)

We analyze the global stability properties of birhythmicity in a self-sustained system with random excitations. The model is a multi-limit-cycle variation in the van der Pol oscillator introduced to analyze enzymatic substrate reactions in brain waves. We show that the two frequencies are strongly influenced by the nonlinear coefficients α and β. With a random excitation, such as a Gaussian white noise, the attractor's global stability is measured by the mean escape time τ from one limit cycle. An effective activation energy barrier is obtained by the slope of the linear part of the variation in the escape time τ versus the inverse noise intensity $1/D$. We find that the trapping barriers of the two frequencies can be very different, thus leaving the system on the same attractor for an overwhelming time. However, we also find that the system is nearly symmetric in a narrow range of the parameters. © *2010 American Institute of Physics*. [doi:10.1063/1.3309014]

Some models employed to describe natural systems, such as, for instance, glycolysis reactions and circadian protein rhythmics, exhibit spontaneous oscillations at two distinct frequencies. The phenomenon is known as birhythmicity, and the underlying dynamical structure is characterized by the coexistence of two stable attractors, each displaying a different frequency. Being the attractors locally stable, the system would however stay at a single frequency, the one selected by the choice of the initial conditions, unless an external source disturbs the evolution and causes a switch to the other attractor. To investigate such process, we have focused on a particular system of biological interest, a modified van der Pol oscillator (that displays birhythmicity), to determine the global stability properties of the attractors under the influence of noise. More specifically, we have characterized the stability of the attractors with the escape times, or the average time that the system requires to switch from an attractor to the other under the influence of random fluctuations. Such analysis reveals that the two attractors can possess very different properties with very different relative residence times. Even excluding the most asymmetric cases, the system can spend something like ten years on one attractor for each second spent on the other. We conclude that although a system can be structurally biorhythmic for the contemporary presence of two locally stable attractors at two different frequencies, actual switch from one frequency to the other could be very difficult to observe. A global stability analysis can therefore help to determine the region of the parameter space in which birhythmic behavior will be genuinely observed.

I. INTRODUCTION

Self-oscillating systems exhibit limit cycles or periodic sustained oscillations. Examples are abundant, with periods ranging from cardiac rhythms of seconds, glycolysis over the minutes, circadian oscillations over the 24 h, while epidemiological oscillations extend even over the years.[1–3] Birhythmicity refers to the coexistence of two attractors characterized by two different amplitudes and two frequencies: depending on the initial conditions, the system can produce self-oscillations at two distinct periods. Such hysteretic behavior has been sometimes observed in biological systems.[4] Many more theoretical studies have shown the possible occurrence of birhythmicity in models of glycolytic oscillations,[5] chemical kinetic equations,[6] circadian protein rhythmics,[7–9] and biochemical reactions.[10] Perhaps the simplest model that exhibits birhythmicity is a variation in the well-known van der Pol oscillator proposed by Kaiser[11] to model enzyme reactions. In such a model it has been shown that two attractors can coexist for some values of the parameters,[11–13] and birhythmicity is robust enough to enable two[14] or more[15] oscillators to synchronize. The aim of this work is to adopt the Kaiser modification of the van der Pol oscillator[11,16,17] as a paradigm for birhythmicity to analyze the global stability properties of the attractors under the influence of random excitations, i.e., the response to finite perturbations.[18–20] In fact while local stability properties that refer to small perturbations of the steady state have been analyzed in Ref. 15, global stability refers to the response to large random fluctuations (large enough to drive the system from one attractor to the other). Such global stability property has not been addressed for the model proposed in Refs. 11–13, and seldom investigated in birhythmic systems (see Ref. 21 for an exception). Global stability is well studied in ac driven (and hence monorhythmical) systems,[19,20,22,23] for

a)Author to whom correspondence should be addressed. Electronic mail: ryamapi@yahoo.fr.

instance, in connection with the phenomenon of stochastic resonance[24] or of switching between chaotic attractors.[25,26] We want here to focus on the passage between two attractors characterized by two different frequencies, and therefore we will emphasize the consequences of noise driven switching on the birhythmic properties, while in periodically driven systems the frequency is preselected by the external drive.

When noise is added, the mean time τ required to escape from a basin of attraction is a useful measure of the attractor's global stability also for nonequilibrium or oscillating systems, such as ac-driven Josephson circuits with intrinsic thermal fluctuations[18] or with finite-spectral-linewidth ac current.[27] In the same spirit, we propose to measure the attractor's global stability with the mean escape time τ from one stable limit-cycle attractor to another stable limit-cycle attractor. Escape occurs when under the influence of a deterministic or random term, the system crosses the boundary of the basin of attraction (i.e., it is driven across the unstable limit cycle).

Let us remark that even if we focus on switches due to random perturbations, one could also drive the system from an attractor to the other by means of a deterministic or structural change. This type of switch will be not considered in the present work; however it is also possible from the deterministic dynamics—considering all possible paths that lead from one attractor to the other with the appropriate noise-dependent weight—to retrieve the escape rate.[18,20,28–30]

We will show that the reason that might hamper the actual observation of birhythmicity in a noisy environment is the asymmetry of the escape times. In such a case the system is likely to stay for a much longer time on one attractor with respect to the other, and therefore one would rarely observe the spontaneous transition from an attractor to the other.[19,20,23] We conclude that although coexistence of two stable attractors with different frequencies is a prerequisite for birhythmicity, actual observation might be hindered by very asymmetric stability properties of the two attractors. In other words we will consider birhythmical systems as bistable systems and the numerically evaluated escape times will serve as a measure of the relative stability of the two solutions. For a glycolytic model it has indeed been proven by means of the Fokker–Planck equation associated with the weak noise limit that the original system with two stable attractors (and hence with birhythmical behavior) changes structures and becomes monorhythmical.[21] Our analysis arrives at a similar conclusion: the escape time from one of the attractors might be very large compared with the escape time of the reverse process, even by many orders of magnitude. In addition, we find that for some range of parameters the system is (approximately) symmetric. In this (indeed narrow) parameter space region the two attractors have comparable properties, and birhythmicity is more likely to be observed.

The paper is organized as follows. In Sec. II, we describe the self-sustained system with random excitation and the algorithm of the numerical simulations. Section III deals with the dynamical attractors of free-noise multi-limit-cycle self-sustained system. We will show that birhythmicity features are not uniform in the parameter region where it appears in the modified van der Pol system. In Sec. IV, we focus on numerical computed escape rates using the Box–Mueller random Gaussian generator algorithm[31] for numerical integration with the Euler method. The Arrhenius factor (i.e., the relation between the escape time τ and the noise intensity D) allows us to determine an effective activation energy barrier ΔU_i, or the slope of the linear part of the variation in the escape time versus the inverse noise intensity, as a useful method to summarize the results. Section V is devoted to conclusions.

II. THE SELF-SUSTAINED SYSTEM WITH RANDOM EXCITATION

A. The multi-limit-cycle van der Pol oscillator

The model considered is a van der Pol-like oscillator with a nonlinear function of higher polynomial order described by the nonlinear equation (overdots as usual stand for the derivative with respect to time)

$$\ddot{x} - \mu(1 - x^2 + \alpha x^4 - \beta x^6)\dot{x} + x = 0, \tag{1}$$

where α, β, and μ are positive parameters that tune the nonlinearity. Model (1) is therefore a prototype for self-sustained systems and exhibits some interesting features of nonlinear dynamical systems; for instance, Refs. 16 and 17 have analyzed the superharmonic resonance structure and have found symmetry-breaking crisis and intermittence. The nonlinear dynamics and the synchronization process of two such systems have been recently investigated in Refs. 13 and 14, while the possibility that introducing an active control of chaos can be tamed for an appropriate choice of the coupling parameters has been considered in Ref. 32.

Equation (1) describes several dynamic systems, ranging from physics to engineering and biochemistry.[33] In particular Eq. (1) seems to be more appropriate for some biological processes than the classical van der Pol oscillator, as shown by Kaiser in Ref. 34. When employed to model biochemical systems, namely, the enzymatic-substrate reactions, x in Eq. (1) is proportional to the population of enzyme molecules in the excited polar state, the quantities α and β measure the degree of tendency of the system to a ferroelectric instability, while μ is a positive parameter that tunes nonlinearity.[13]

The nonlinear self-sustained oscillator equation (1) possesses more than one stable limit-cycle solution,[34] a condition for the occurrence of birhythmicity. Birhythmic systems are of interest, for example, in biology to describe the coexistence of two stable oscillatory states, a situation that can be found in some enzyme reactions.[35] Another example is the explanation of the existence of multiple frequency and intensity windows in the reaction of biological systems when they are irradiated with very weak electromagnetic fields.[17,34,36–39] In this work we will focus on model (1) as a prototype for the occurrence of birhythmicity.

B. The model with random excitation and algorithm for numerical simulations

Let us consider the multi-limit-cycle van del Pol-like oscillator equation (1) to model coherent oscillations in biological systems, such as an enzymatic substrate reaction with ferroelectric behavior in brain waves models (see Refs.

11–13 for more details). In this case, one should include the electrical field applied to the excited enzymes, which depends, for example, on the external chemical influences (i.e., the flow of enzyme molecules through the transport phenomena). One can therefore assume that the external chemical influence contains a random perturbation. Therefore, adding both the chemical and the dielectric contribution, the activated enzymes are subject to a random excitation governed by the Langevin version of Eq. (1), namely,

$$\ddot{x} - \mu(1 - x^2 + \alpha x^4 - \beta x^6)\dot{x} + x = \Gamma(t), \tag{2}$$

where $\Gamma(t)$ is a Gaussian additive white noise[40] whose statistical features are completely determined by the additional properties

$$\langle \Gamma(t) \rangle = 0, \quad \langle \Gamma(t)\Gamma(t') \rangle = 2D\delta(t - t'). \tag{3}$$

The white-noise quality of Γ is contained in the Dirac δ-function correlation (3). The parameter D is the intensity of the Gaussian white noise.

In this work we will numerically integrate Eqs. (2) and (3) using a Box–Mueller algorithm[31] to generate the Gaussian white noise from two random numbers a and b, which are uniformly distributed on the unit interval [0,1]. By introducing the new variable $\dot{x}=u$, Eq. (2) can be written in the form

$$\dot{x} = u, \tag{4a}$$

$$\dot{u} = \mu(1 - x^2 + \alpha x^4 - \beta x^6)u - x + \Gamma. \tag{4b}$$

The simple Euler algorithm version of the integration of Eq. (4a) is given by

$$\Gamma_{\Delta t} = \sqrt{-4D\Delta t \log(a)}\cos(2\pi b), \tag{5a}$$

$$x|_{t+\Delta t} = x + u\Delta t, \tag{5b}$$

$$u|_{t+\Delta t} = u + (\mu(1 - x^2 + \alpha x^4 - \beta x^6)u - x)\Delta t + \Gamma_{\Delta t}. \tag{5c}$$

The step size used for numerical integration is generally equal to $\Delta t=0.0001$, but in some cases we have used a smaller step. We have also checked that averaging over as many as 200 realizations the results converge within few percents. We notice that there are more accurate methods to estimate the escape from a basin of attraction, or, in general, close to an absorbing barrier, to avoid the inaccuracy due to a finite sampling of the random evolution.[41] However, we have carefully checked that the results we have obtained are independent of the step size. This has been done in two ways: halving the step size until stable results are reached (and with much attention to low noise intensity D[41]) and calibrating the numerical method with a potential with a well-defined activation barrier to retrieve the Kramer escape rate.[42]

So, although analytical treatments based on the Fokker–Planck version of the Langevin equation (2),[43] the variational approach,[18,20,28–30] or faster numerical algorithms such as the stochastic version of the Runge–Kutta methods are available, we have preferred to use the simple procedure given by Eq. (5a) that proved fast enough for the present project.

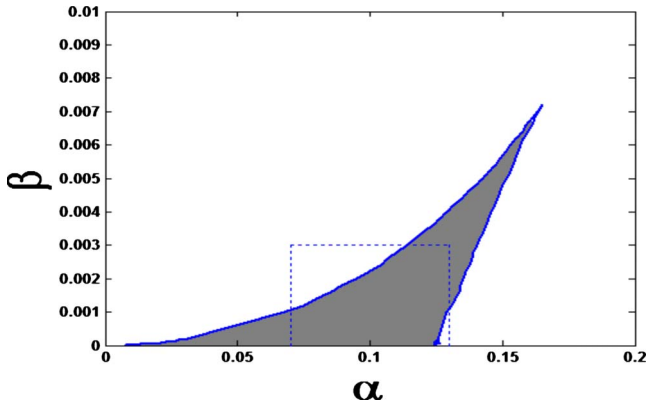

FIG. 1. (Color online) Parameter domain for the existence of a single limit cycle (white area) and three limit cycles (gray area) with $\mu=0.1$. The bifurcation line on the left denotes the saddle-node bifurcation of the outer or large amplitude cycle (see Fig. 2), while the right-hand side contour marks the saddle-node bifurcation of the inner cycle. The rectangle denotes the parameter region in Table II.

In the absence of noise ($\Gamma=0$), Eq. (2) reduces to the modified version of the van der Pol oscillator [see Eq. (1)], which has steady-state solutions that correspond to attractors in state space and depend on the parameters α, β, and μ. Before taking up the subject of noise-induced transitions between dynamical attractors, we focus on Sec. III on the state-space structure of the attractors and basin boundaries in the noise-free self-sustained system. We will show that the features of birhythmicity in this modified van der Pol oscillator strongly depend on α and β.

III. DYNAMICAL ATTRACTORS AND BIRHYTHMICITY PROPERTIES

In this section we summarize the dynamical attractors of the modified van der Pol model (1) without Gaussian noise. The periodic solutions of Eq. (1) can be approximated by

$$x(t) = A\cos\Omega t. \tag{6}$$

We recall that approximated analytic estimates of the amplitude A and the frequency Ω have been derived from Ref. 13, and it has been found that the amplitude A is independent of the coefficient μ, which only enters in the frequency Ω.

It appears that depending on the values of the parameters β and α, the modified van der Pol equation (1) possesses one or three limit cycles. When three limit cycles are obtained, two of them are stable and one is unstable, a condition for birhythmicity; the unstable limit cycle represents the separatrix between the basins of attraction of the two stable limit cycles. We show in Fig. 1 the bifurcation lines that contour the region of existence of birhythmicity in the two parameter phase space (β-α).[13,14] The bifurcation line on the left denotes the passage from a single limit cycle to three limit cycles, while the right line denotes the reverse passage from three limit cycles to a single solution. At the conjunction, a codimension-two bifurcation, or cusp,[43] appears. The first bifurcation encountered increasing α corresponds to the saddle-node bifurcation of the outer or larger amplitude cycle, while the second bifurcation occurs in correspondence of a saddle-node bifurcation of the inner or smaller ampli-

TABLE I. Comparison between analytical and numerical characteristics of the limit cycles. All data refer to the case $\mu=0.1$.

$S_i=(\alpha,\beta)$	Analytical amplitude	Numerical amplitude	Analytical frequency	Numerical frequency
$S_1=(0.114;0.003)$	$A_1=2.377\ 20$	$A_1=2.378$	$\Omega_1=1.002\ 12$	$\Omega_1=1.000\ 15$
	$A_2=5.026\ 38$	Unstable	$\Omega_2=1.001\ 13$	Unstable
	$A_3=5.466\ 65$	$A_3=5.464$	$\Omega_3=1.0231$	$\Omega_3=1.019\ 575$
$S_2=(0.1;0.002)$	$A_1=2.3069$	$A_1=2.302\ 65$	$\Omega_1=0.987$	$\Omega_1=0.988$
	$A_2=4.8472$	Unstable	$\Omega_2=1.000\ 113$	Unstable
	$A_3=7.1541$	$A_3=7.1345$	$\Omega_3=0.971\ 23$	$\Omega_3=0.978\ 31$
$S_3=(0.12;0.003)$	$A_1=2.4269$	$A_1=2.4259$	$\Omega_1=0.985$	$\Omega_1=0.988$
	$A_2=4.2556$	Unstable	$\Omega_2=0.999$	Unstable
	$A_3=6.3245$	$A_3=6.339\ 18$	$\Omega_3=0.9865$	$\Omega_3=0.988$
$S_4=(0.13;0.004)$	$A_1=2.4903$	$A_1=2.489\ 71$	$\Omega_1=1.000\ 212$	$\Omega_1=1.000\ 507$
	$A_2=4.4721$	Unstable	$\Omega_2=1.000\ 113$	Unstable
	$A_3=5.0791$	$A_3=5.077\ 39$	$\Omega_3=0.999\ 12$	$\Omega_3=0.9989$
$S_5=(0.145;0.005)$	$A_1=2.6605$	$A_1=2.659\ 63$	$\Omega_1=1.000\ 212$	$\Omega_1=1.000\ 507$
	$A_2=3.8305$	Unstable	$\Omega_2=1.000\ 113$	Unstable
	$A_3=4.964$	$A_3=4.963\ 36$	$\Omega_3=1.000\ 499\ 03$	$\Omega_3=1.000\ 256$
$S_6=(0.154;0.006)$	$A_1=2.7864$	$A_1=2.785\ 32$	$\Omega_1=0.999\ 23$	$\Omega_1=0.9989$
	$A_2=3.8821$	Unstable	$\Omega_2=1.000\ 113$	Unstable
	$A_3=4.2698$	$A_3=4.268\ 07$	$\Omega_3=1.000\ 231$	$\Omega_3=1.000\ 507$

tude cycle. The two frequencies associated with the limit cycles are very similar close to the lowest α bifurcation and clearly distinct at the highest α bifurcation line, as will be discussed later in detail.

Table I provides for some selected sets S_i of the parameters in the domain of existence of three limit cycles on which we will focus our attention the comparison between amplitudes and frequencies derived from the analytical estimate of Ref. 13 and from numerical simulations of Eq. (1). From the table it is clear that birhythmicity is indeed present—the two stable attractors are characterized by different frequencies. However, the two frequencies are very similar, and in practice it might prove very difficult to resolve the difference. To illustrate the dynamics of the self-sustained oscillations, we report in Fig. 2 the limit cycles and in Figs. 3 and 4 the time dependent oscillations. In Fig. 3, the two frequencies are very similar, while in Fig. 4 we report the case of two clearly distinct frequencies. It is clear that for the slow oscillations (the solid line in Fig. 4), the behavior is not well approximated by the sinusoidal approximation (6). It can also be noticed that the amplitude is still captured by the theory, while the agreement between the predicted and the observed frequency becomes poor at low frequencies. In fact, for Fig. 4(i), $\alpha=0.12$, $\beta=0.0014$, the theoretical analysis[13] predicts $A_1=2.49$ and $A_3=10.89$ with frequencies $\Omega_1=0.999$ and $\Omega_3=0.532$, respectively, in good agreement with the numerical data $\Omega_1=1.00$ and $\Omega_3=0.516$. For the case of Fig. 4(ii), $\alpha=0.13$, $\beta=0.001$, the theoretical analysis[13] gives $A_1=2.828$ and $A_3=13.84$ with frequencies $\Omega_1=0.998$ and $\Omega_3=0.521$, while the numerical data read $\Omega_1=1.00$ and $\Omega_3=0.195$. It is evident that the observed frequency of the large cycle, 0.195, is much less than the predicted value of 0.521.

In order to understand the effect of the parameters α and β on the dynamical states, we have simulated Eq. (1) to numerically derive the frequencies Ω_i; the results are shown in Table II. For α and β in the white area of Fig. 1, there exists only a single limit-cycle solution. In the gray area of Fig. 1 there are multi-limit-cycle solutions with $\Omega_1\neq\Omega_3$. Figure 5 shows the dependence of the frequencies Ω_i versus the coefficient β when the parameter α is fixed. In this parameter region for each value of α, the two limit-cycle frequencies are different at low β values (see Fig. 4), but converge to the same frequency when β increases (see Fig. 3). This reveals that the saddle-node bifurcation at the upper boundary of the multi-limit-cycle area in Fig. 1 occurs when the two frequencies are very similar. Thus we conclude that birhythmicity smoothly disappears increasing β because the two frequencies become undistinguishable, while the attractors are clearly distinct at the saddle-node bifurcation.

Figure 6 shows the dependence of Ω_i versus α for different values of β. As α increases, we move from the boundaries of the multi-limit-cycle area where $\Omega_1=\Omega_3$ to enter the region of the map in which the two limit-cycle frequencies are different (i.e., $\Omega_1\neq\Omega_3$).

So we conclude that the saddle-node bifurcation at the right-hand side refers not only to the appearance of a new limit cycle, but also to a cycle with a definitely different frequency, and therefore in this region birhythmicity is more easily observed. In contrast, it is evident that it will be extremely difficult to detect birhythmicity for low α.

IV. NUMERICAL ESTIMATE OF ESCAPE RATES AND GLOBAL STABILITY ANALYSIS

A. Escape times from the periodic attractors

At nonzero noise intensity ($D\neq 0$), the random force causes the system to occasionally jump from one limit cycle to the other. The system initialized on a given limit-cycle attractor (with amplitude A_1 or A_3) is forced by the random fluctuations of the Γ term in Eq. (2) to leave the attractor and to wander about in the neighboring state space. Escape oc-

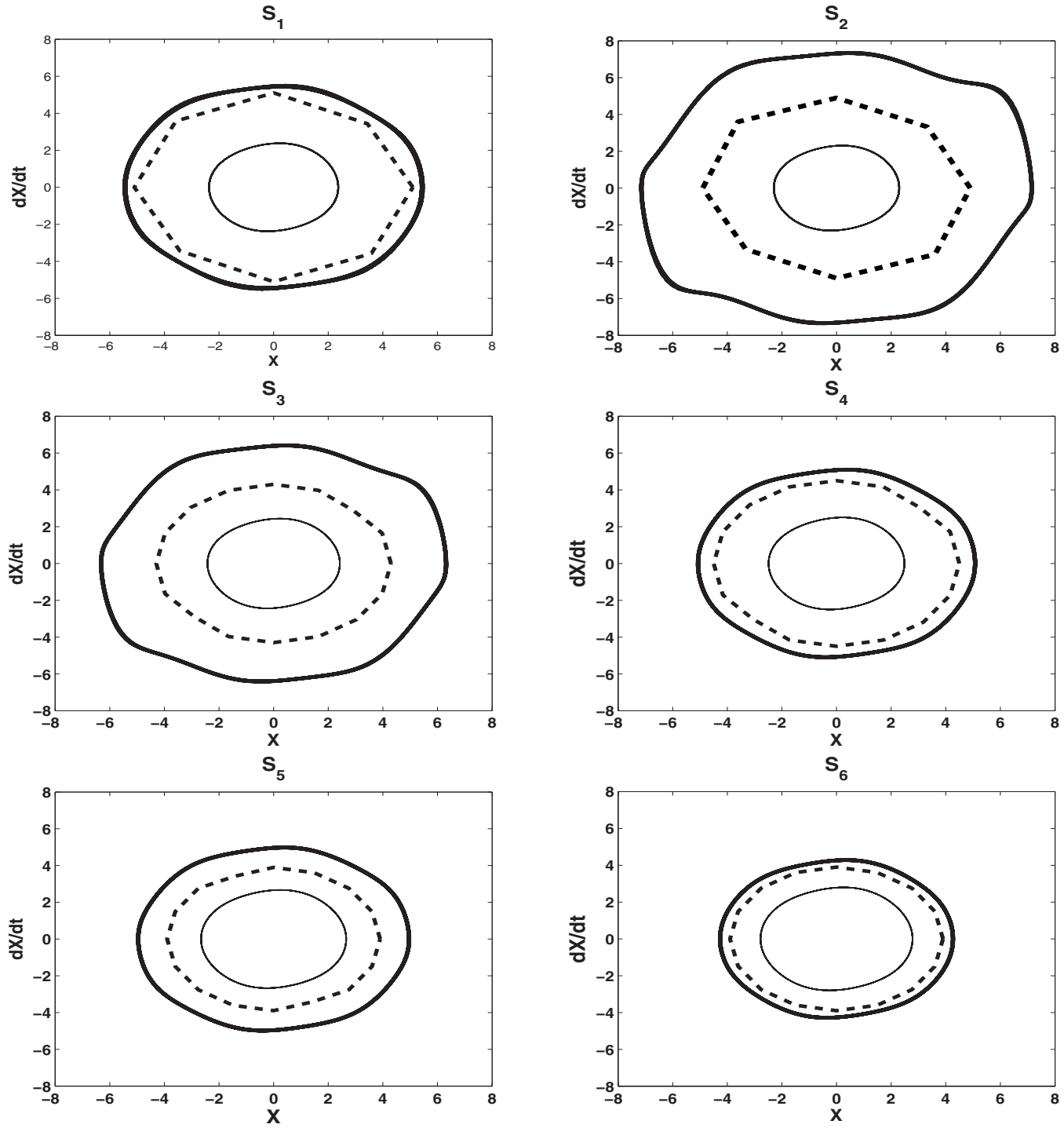

FIG. 2. The two stable coexisting limit-cycle attractors obtained by numerical integration of Eq. (1) for $\mu=0.1$ and the sets of parameters S_i (see Table I). The thin line refers to the attractor of smaller amplitude (A_1) and the thick line to the larger amplitude (A_3). The dashed line denotes the unstable limit cycle and separates the basin of attraction of the inner or smaller amplitude cycle from the basin of attraction of the outer or larger amplitude cycle.

curs when this random motion drives the system across the boundary of the basin of attraction (i.e., across the unstable limit cycle with amplitude A_2). The mean time τ required for escape from a basin of attraction is a useful measure of the attractor's global stability. This escape time is analogous to the escape time of a system trapped in a minimum of the effective potential, and the escape implies that the random force drives the system to the other minimum of the effective potential. The activation energies shown in Fig. 7 sketch the escape process to be considered in Sec. IV B. In fact, there are two metastable states.

(1) The system is trapped at the effective potential minimum in the basin of attraction of the limit-cycle amplitude A_1. Then, escape to the basin of attraction with limit-cycle amplitude A_3 occurs when the system under

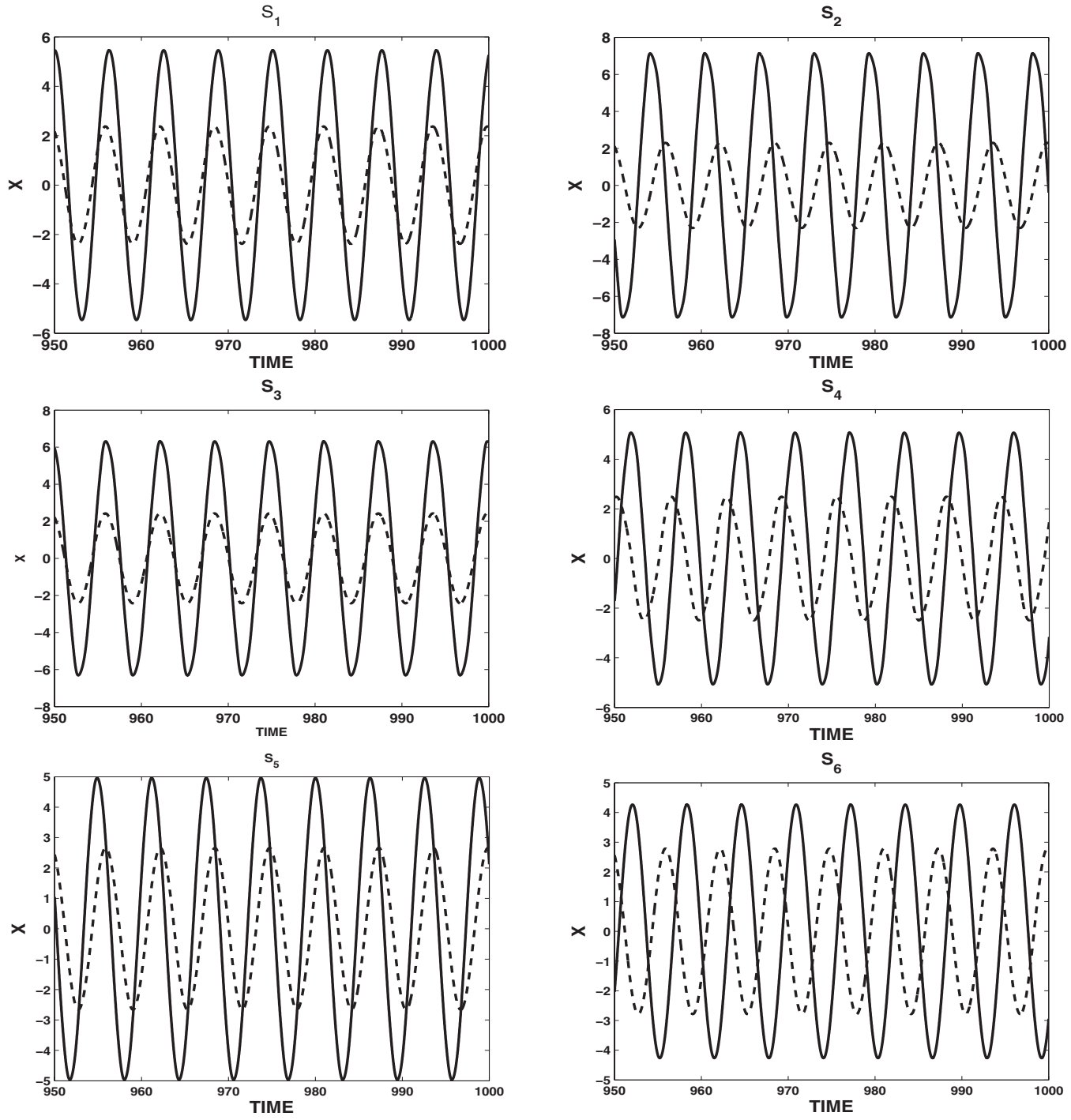

FIG. 3. The coexistence between two regimes of noise-free self-sustained oscillations corresponding to the larger (solid line, A_3, and frequency Ω_3) and smaller (dotted line, A_1, and frequency Ω_1) limit cycles, the two frequencies are approximately the same, $\Omega_1 \simeq \Omega_3$. The set of parameters is the same as for the attractors shown in Fig. 2, see Table I.

Gaussian white noise crosses the unstable limit-cycle amplitude A_2 (i.e., $|x|>A_2$). This can be numerically computed by choosing the initial conditions close to the origin. Thus, the corresponding effective energy barrier to escape from the basin of attraction with limit-cycle amplitude A_1 to the one with amplitude A_3 is called ΔU_1.

(2) In the reverse situation, the system is trapped at the effective potential minimum in the basin of attraction of the limit-cycle amplitude A_3. The initial conditions are chosen outside the basin of attraction of the limit cycle A_1 and far of the unstable limit cycle A_2. We will denote with ΔU_3 the effective energy barrier to escape from the basin of attraction with limit-cycle amplitude A_3 across the unstable limit cycle with amplitude A_2 (i.e., $|x|<A_2$) toward the limit cycle with amplitude A_1.

Figure 7 sketches our notation and the most relevant cases.

- Case (i): Fig. 7(i) corresponds to the case where ΔU_1 is larger than ΔU_3. We shall see that ΔU_1 can become very

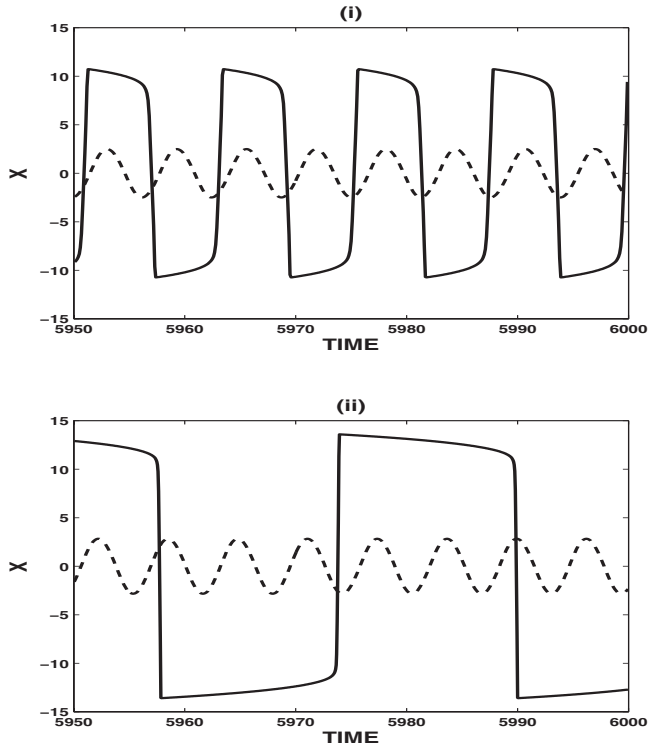

FIG. 4. Birhythmicity with oscillations at two clearly different frequencies, $\Omega_1=2\Omega_3$. (i) $(\alpha;\beta)=(0.12;0.0014)$ and (ii) $(\alpha;\beta)=(0.13;0.001)$. In both figures we have set $\mu=0.1$.

large (depending on the coefficients α and β); in such conditions the attractor of the limit-cycle amplitude A_1 is much more stable than the limit-cycle amplitude A_3. Thus, the system is more likely to stay on the limit-cycle attractor A_1.

- Case (ii): Fig. 7(ii) depicts the symmetric case $\Delta U_1 \simeq \Delta U_3$. Both attractors are equivalent and we are in a symmetric bistable double well. The system has approximately the same probability to stay in one or the other basins.
- Case (iii): Fig. 7(iii) shows the case where the energy barrier ΔU_1 is less than ΔU_3. Here is the reverse situation of the case (i), and the first attractor is less stable. The system is more likely to stay on the limit-cycle attractor A_3.

Thus, while in principle, bistability occurs for all values of the parameters α and β in the gray area of Fig. 1, noise driven bistability is more likely to be observed in a narrower region of the parameter space, see case (ii).

B. Numerical estimate of the escape rates and effective energy barriers

Although there exists a method for the calculation of activation energies in nonequilibrium systems that do not admit a bona fide potential using the principle of minimum available noise energy,[18–20,28–30] we adopt here the indirect approach of computing the escape time and then we infer on the values of the activation energies. The mean escape time τ is computed as the average over a series of trials of the time τ_i required for the system to move from one attractor to the other attractor under the influence of noise. For each trial, integration is begun at $t=0$ with the system initialized on the attractor and proceeds by numerically solving the system equations with a finite difference integration method of step size Δt [see Eq. (5a)]. The fact that the random motion of the system is due to a Gaussian white noise ensures that escape will occur with probability 1 within a finite time.[18] Thus, the main question is how long the system stays in the same basin of attraction. We expect that the escape time is given by the inverse Kramer escape rate or from the Arrhenius factor[42]

$$\tau \simeq \exp(\Delta U_i/D), \tag{7}$$

where $\Delta U_i (i=1,3)$ is the difference between maximum and minimum values of an effective potential.

We remark that a function plays the role of a thermodynamic potential for fluctuating dissipative systems that do not possess a bona fide potential[30] if it correctly describes the

TABLE II. Dependence of the energy barriers ΔU_i in the parameters plane (α,β) with $\mu=0.1$.

	$\alpha=0.07$	$\alpha=0.08$	$\alpha=0.09$	$\alpha=0.1$	$\alpha=0.12$	$\alpha=0.13$
$\beta=0.004$						$\Delta U_1=0.074$
						$\Delta U_3=0.0072$
$\beta=0.003$					$\Delta U_1=0.095$	$\Delta U_1=0.028$
					$\Delta U_3=1.656$	$\Delta U_3=0.0075$
$\beta=0.0025$					$\Delta U_1=0.054$	$\Delta U_1=0.015$
					$\Delta U_3=2.7$	$\Delta U_3=6.75$
$\beta=0.002$				$\Delta U_1=0.25$	$\Delta U_1=0.035$	$\Delta U_1=0.0097$
				$\Delta U_3=0.75$	$\Delta U_3=10.5$	$\Delta U_3=28.8$
$\beta=0.0016$			$\Delta U_1=0.45$	$\Delta U_1=0.183$	$\Delta U_1=0.026$	$\Delta U_1=0.0035$
			$\Delta U_3=0.93$	$\Delta U_3=7.78$	$\Delta U_3=68.2$	$\Delta U_3=224$
$\beta=0.0014$		$\Delta U_1=0.98$	$\Delta U_1=0.34$	$\Delta U_1=0.16$	$\Delta U_1=0.021$	$\Delta U_1=0.0017$
		$\Delta U_3=0.014$	$\Delta U_3=3.78$	$\Delta U_3=16.14$	$\Delta U_3=152.3$	$\Delta U_3=233.5$
$\beta=0.0012$		$\Delta U_1=0.62$	$\Delta U_1=0.291$	$\Delta U_1=0.13$	$\Delta U_1=0.104$	$\Delta U_1=0.0015$
		$\Delta U_3=2.15$	$\Delta U_3=11.6$	$\Delta U_3=17.5$	$\Delta U_3=308$	$\Delta U_3=791$
$\beta=0.0011$		$\Delta U_1=0.65$	$\Delta U_1=0.28$	$\Delta U_1=0.123$	$\Delta U_1=0.015$	$\Delta U_1=0.003$
		$\Delta U_3=4.35$	$\Delta U_3=27.5$	$\Delta U_3=104.9$	$\Delta U_3=564$	$\Delta U_3>1000$
$\beta=0.001$	$\Delta U_1=1.3$	$\Delta U_1=0.52$	$\Delta U_1=0.25$	$\Delta U_1=0.11$	$\Delta U_1=0.014$	$\Delta U_1=0.0001$
	$\Delta U_3=0.53$	$\Delta U_3=10.7$	$\Delta U_3=16.05$	$\Delta U_3=105.6$	$\Delta U_3>1000$	$\Delta U_3>1000$

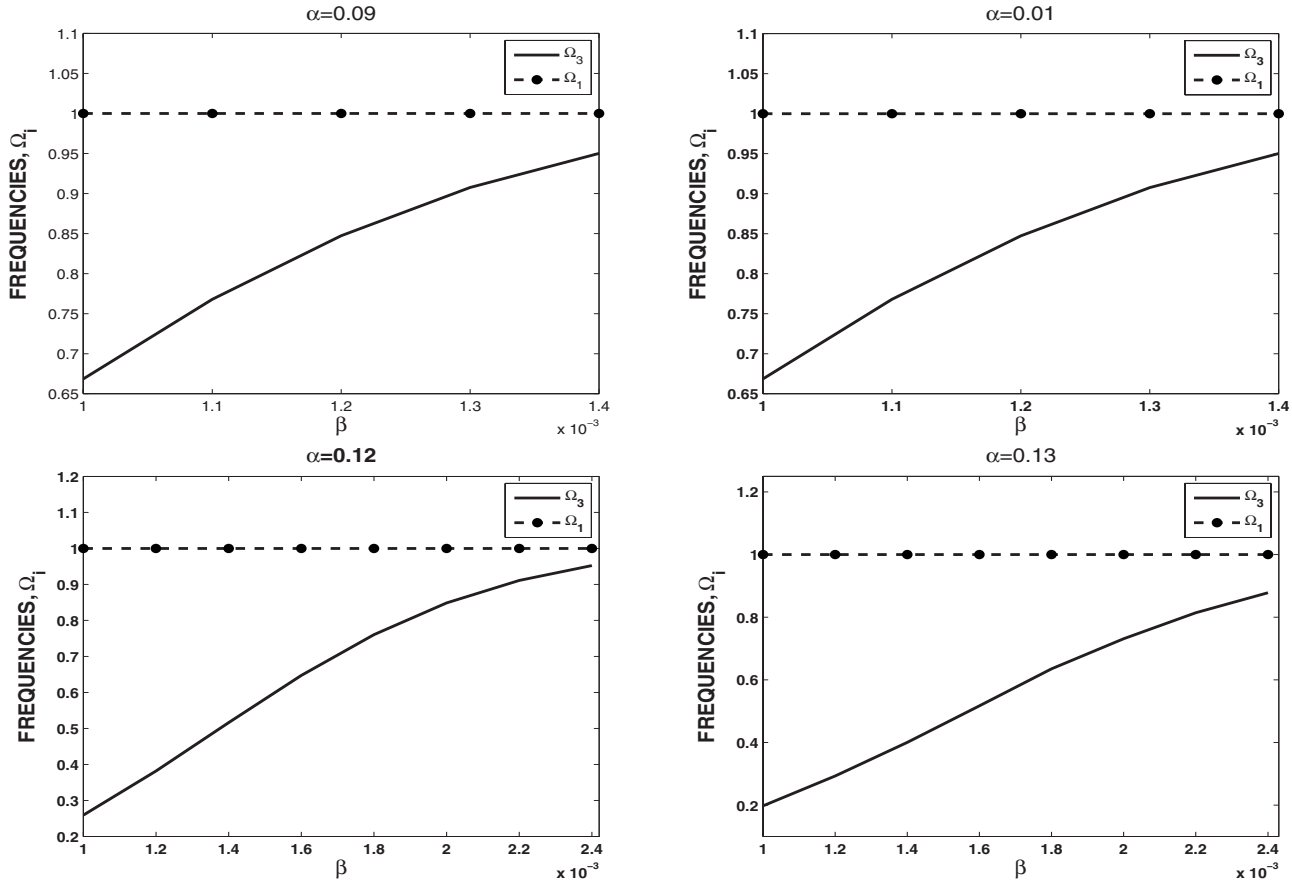

FIG. 5. Frequency Ω_i vs the parameter β for different values of α for the noise-free self-sustained system. The nonlinear parameter reads $\mu=0.1$.

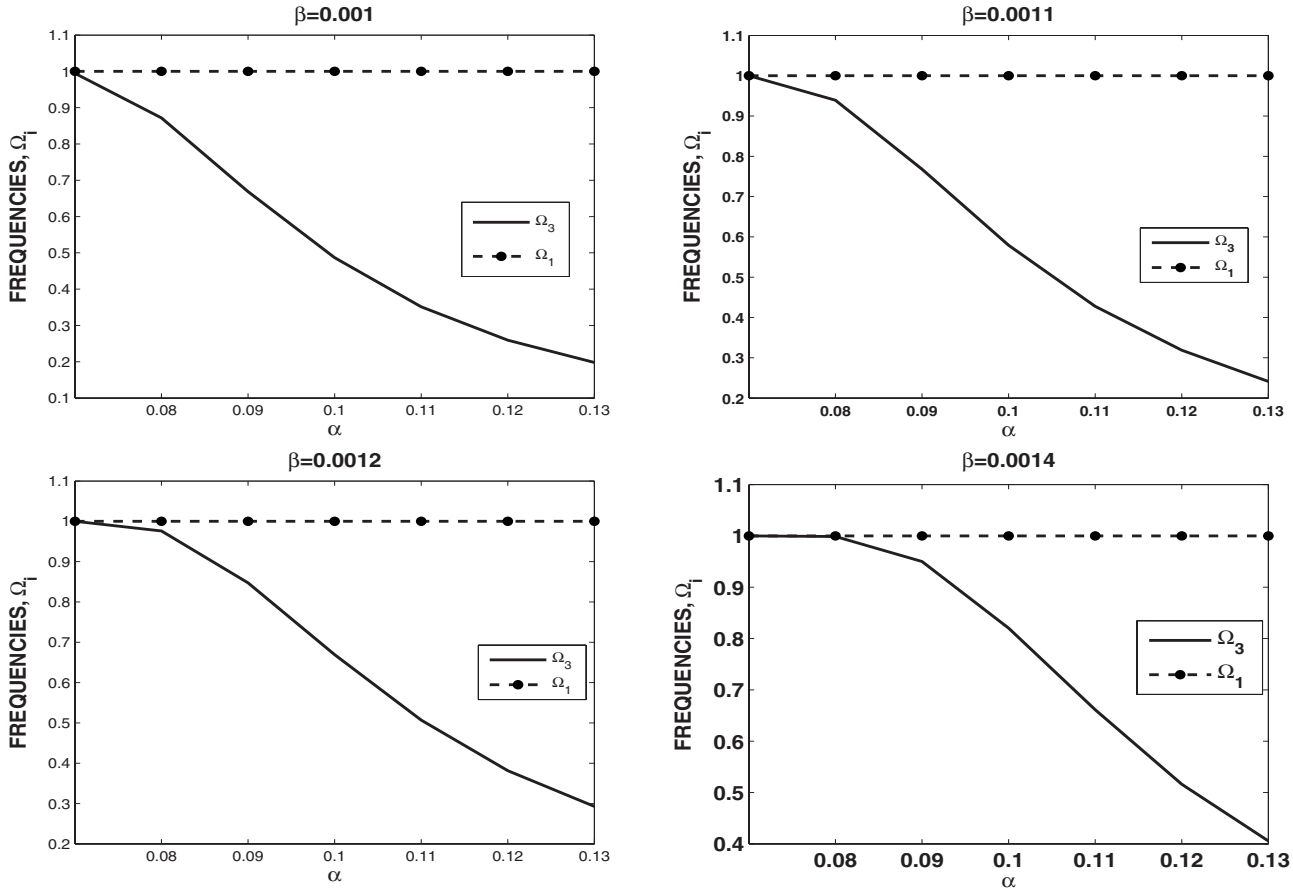

FIG. 6. Frequency Ω_i vs the parameter α for different values of β for the noise-free self-sustained system. The nonlinear parameter reads $\mu=0.1$.

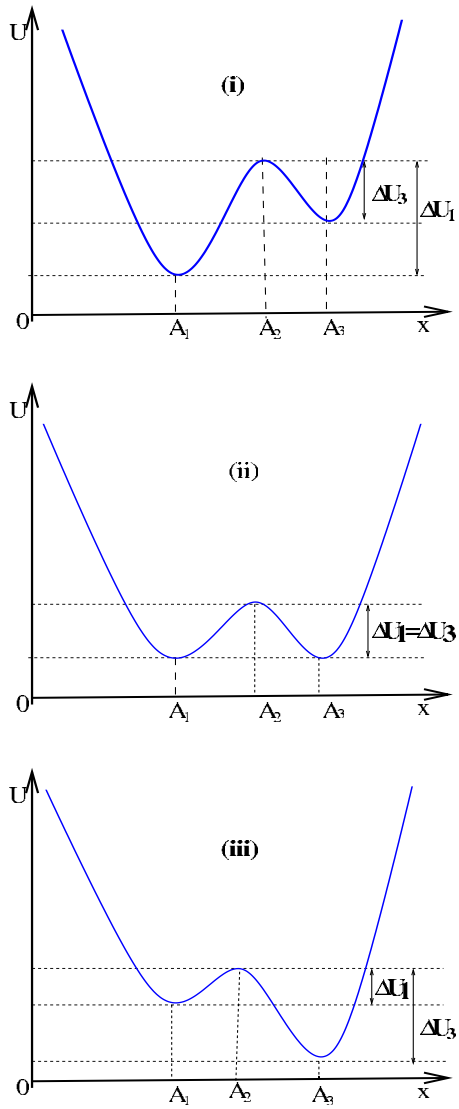

FIG. 7. (Color online) Sketch of the effective activation energies ΔU_1 and ΔU_3 for the free-noise self-sustained oscillator with multilimit cycles. We underline that the barrier height has a clear meaning as the slope of the escape time 7, while the effective potential U is qualitatively drawn only to help the intuition.

asymptotic response to noise. In a sense, one reverses the Kramer logic: it is called effective potential a function U that gives the slope of the logarithm of the escape time versus the inverse of the noise intensity for low noise strength [see Eq. (7)]: $U \propto \log(\tau/D)$ (for $D \to 0$). In this framework, one could regard the potential U as a way to summarize the behavior of the escape times. In other words it is completely equivalent either to say that the escape times are exponentially distributed versus the inverse of the noise (for low noise) with slope U or that the effective potential reads U.

The relevant attractors and basins of attraction are those shown in Fig. 2. The data show that the mean escape times τ obtained from simulations for both limit-cycle state A_1 and A_3 state increase exponentially with the inverse noise intensity. With the parameter sets S_i, we find that the variation in the average escape time (on a logarithm scale) as function of the inverse noise intensity $1/D$ strongly depends on the nonlinear coefficients α and β. For example, the sets S_1, S_4, and S_6 correspond to case (i) in which the attractor of the limit cycle A_3 is less stable than the attractor A_1. The symmetric bistable situation, case (ii), is observed with the set S_5. The last case (iii) is found for the sets S_2 and S_5. It is important to note that case (ii) only occurs in a very narrow range, $0.08 < \alpha < 0.09$ and $0.0012 < \beta < 0.0014$.[19,20] Outside this narrow area the properties of the two attractors are very different.

Fitting a straight line through the data points in the linear part of Eq. (7) and measuring its slope, we obtain an estimate of ΔU_1 and ΔU_3, the effective activation energies for the escape from the limit-cycle attractors A_1 and A_3, respectively. Since the effective activation energy is defined by the low-noise intensity asymptote, the accuracy of numerical simulation estimates can be affected if high-noise intensity points (i.e., points where the relation is not linear) are included in the fitting procedure. For this reason, data points for which the resulting Arrhenius factor bends have been excluded from the fitting procedure (we employ a χ^2 test to check for linearity). Figure 8 shows the variation in the effective energy barriers versus the coefficient μ with the set of parameters S_i. The effective energy barriers increase when μ increases, and the behaviors strongly depend upon the set of the parameters S_i. The scenarios mentioned in Sec. IV B can be found in the behaviors of $\Delta U_{1,3}$ [i.e., cases (i), (ii), and (iii)]. Case (i) appears in Fig. 8 for the sets S_1, S_4, S_6, in which the energy barrier ΔU_1 quickly increases. Here, one concludes that the limit-cycle attractor A_1 of the modified van der Pol oscillator is much more stable than the attractor A_3 (with respect to Gaussian white noise). The system will likely stay for a long time in the effective potential well of the limit-cycle attractor A_1, for the corresponding effective barrier is higher. For instance when $\mu = 0.5$ in S_1, we observe $\Delta U_1 / \Delta U_3 \simeq 80$. The set S_5 corresponds to the almost symmetric bistable situation, i.e., case (ii). Both effective energy barriers ΔU_1 and ΔU_3 increase when μ increases and are comparable: the system remains for approximately the same time in the two effective potential wells. In the last scenario S_2 and S_3, i.e., case (iii), we have a phenomenon opposed to that of case (i): the limit-cycle attractor A_3 is much more stable than the attractor A_1. The system remains for a much longer time in the limit-cycle attractor A_3 because the energy barrier is too high, so if the noise level is large enough to cause a switch from A_3 to A_1, the same noise will drive back the system to A_3 in a very short time interval with very high probability.

Let us remark that "short" and "long" might be very different.[19,20,23] To measure the different properties, we compute the average persistence or residence time $P_{1,3}$ on the attractor with limit-cycle amplitude $A_{1,3}$ as

$$P_j = \frac{\tau_j}{\tau_1 + \tau_3}, \quad j = 1,3, \tag{8}$$

where $\tau_{1,3}$ is the escape time from the first attractor A_1 or third attractor A_3, see Eq. (7). For the parameters S_1, for noise intensity around $D = 1/20$, we get $P_3 = 0.018$, and obviously $P_1 = 0.982$, i.e., the system will spend 1.8% of the time on the third attractor A_3 and 98.2% on the first attractor A_1.

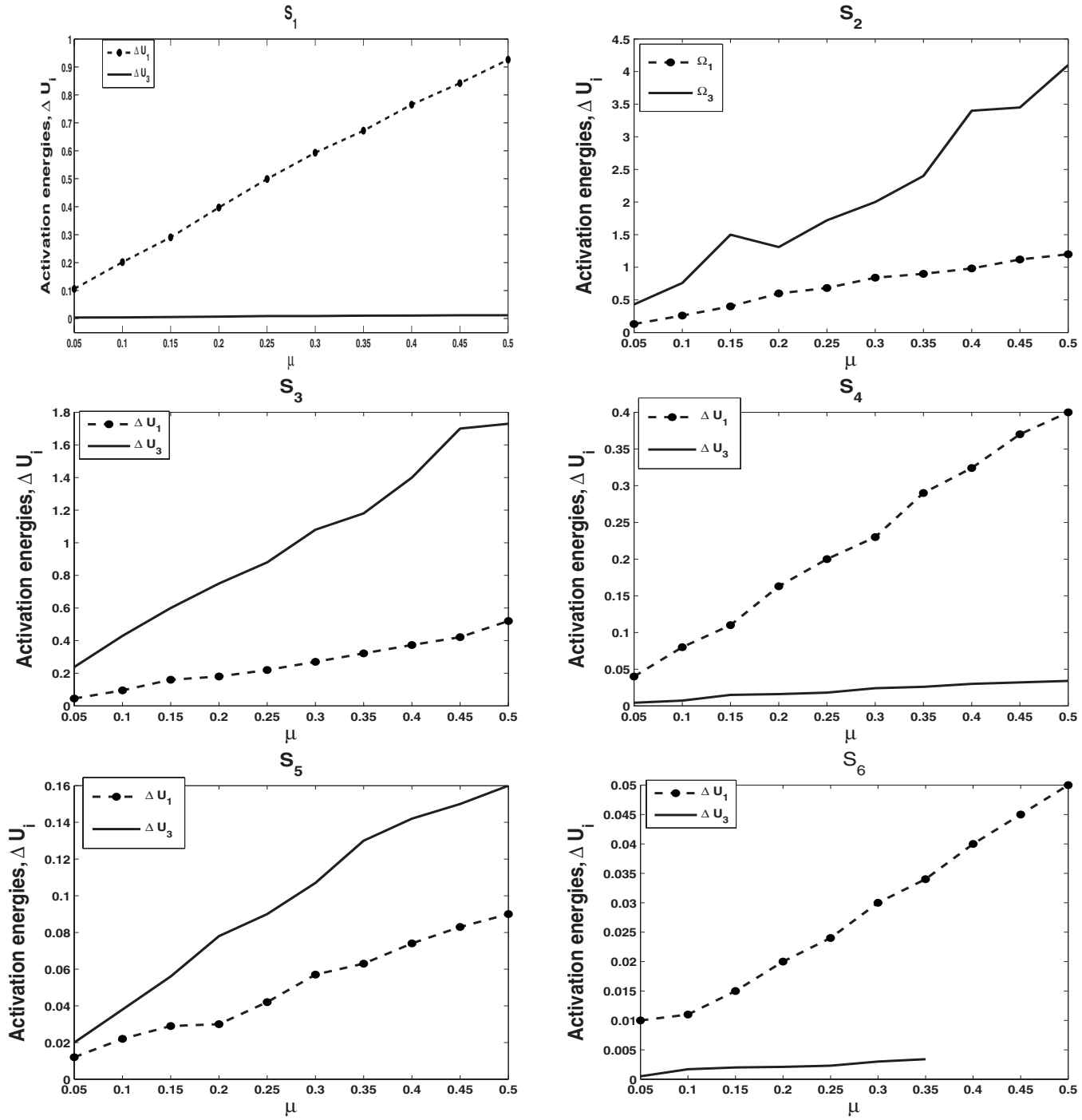

FIG. 8. Effective activation energies vs the coefficient μ with the set of parameters S_i. The thick line corresponds to escape from the outer cycle A_3, while the dashed line refers to escape from the inner cycle A_1. The parameters α and β are the same as in Table I.

Decreasing the noise down to $D=1/100$, P_3 decreases to $P_3 \simeq 3\times 10^{-9}$. In other words, for any second spent on the less stable attractor A_3 the system will stay for about ten years on the most stable state A_1. Such a dramatic change at low noise occurs for $\Delta U_1/\Delta U_3 \simeq 50$. From Table II it is clear that the ratio between energy barriers can easily be much larger.

To analyze the dynamic structure in the various areas of the chart drawn from Fig. 1, we present in Table II the effective energy barriers as a function of the coefficients α and β selected in the dotted rectangle of Fig. 1. When β is fixed and α increases, the effective energy barrier ΔU_1 decreases, whereas the energy barrier ΔU_2 considerably increases. For example, for $\beta=0.0014$, the effective energy barrier of the limit-cycle attractor A_1 decreases from $\Delta U_1(\alpha=0.08)=0.98$ to the value $\Delta U_1(\alpha=0.13)=0.0017$, while the barrier ΔU_3 increases from $\Delta U_3(\alpha=0.08)=0.014$ to the value $\Delta U_3(\alpha=0.07)=233.5$. Then, there is a high probability that the system remains for a longer time in the limit-cycle attractor A_3, see Eq. (7). A similar behavior is reported when α is

fixed and that β increases. Let us note about Table II that for low β value and high α values, case (iii) becomes predominant: ΔU_3 increases and becomes so large that we have not been able to compute such a barrier even with simulations as long as $t_{max} \simeq 10^{10}$ normalized units. We can only estimate the barrier to be larger than 1000.

The behavior of the effective energy barriers can be also interpreted in the following manner: the right side of the gray area of the existence of bistable regime in Fig. 1, where the two frequencies are clearly different, corresponds to the physical case where one of the two limit-cycle attractors, namely, A_3, has a very high effective activation energy, while the other, namely, A_1, vanishes because the effective potential barrier becomes zero. This process explains the passage from birhythmicity to a single limit-cycle attractor.

V. CONCLUSIONS

We have considered the characteristics of birhythmicity and the global stability properties of the attractors in a self-sustained system. We have found that birhythmicity in a modified van der Pol oscillator is strongly influenced by the nonlinear coefficients α and β: the two frequencies converge or diverge when the nonlinear coefficients are varied, leading to almost undistinguishable frequencies for low α and high β. Adding a random excitation, we have found that the system crosses the boundary between the basins of attraction (i.e., moves across the unstable limit cycle with amplitude A_2). The mean time τ to escape from one limit-cycle attractor to the other has been estimated in the low-noise limit, and it is proposed as a measure of the attractor's global stability. By considering the variation in the mean escape time τ versus the inverse noise intensity $1/D$, the slope of the linear part has enabled us to summarize the results in the form of an effective activation energy barrier, which is function of the physical system parameters. We have found that as in other systems that exhibit noise induced switches between two attractors, the escape times can be very different,[19,20,23] so it could be difficult to observe birhythmicity for high α and low β. We remark that systems[19,20,23] are periodically driven, and therefore monorhythmic.

We conclude that although birhythmicity per se refers just to the occurrence of two frequencies, actual observation is subject to much more restrictive conditions. Our purpose is to go beyond the mere existence of birhythmicity to show that there are limitations that restrict the likeliness that birhythmicity spontaneously occurs. We speculate that there might be other models that do possess two attractors with different frequencies, but noise driven birhythmicity is difficult to observe because of the different stability properties of the attractors. This might be the reason why birhythmicity has been predicted in many models, but rarely observed in experiments—actually there is to our knowledge just one case of clear observation of birhythmic behavior.[4] Moreover, the switch from an attractor to another in Ref. 4 is due to a change in the parameters, not to spontaneous transition from a frequency to the other. We suggest that an analysis similar to that carried out in this work is therefore useful to ascertain the birhythmic property in a real system.

ACKNOWLEDGMENTS

R.Y. undertook this work with the support of the ICTP (International Centre for Theoretical Physics) Programme for Training and Research in Italian Laboratories, Trieste, Italy. He also acknowledges the support of the Laboratorio Regionale CNR/INFM, Superconducting Materials, Salerno, Italy.

[1] A. Goldbeter, *Biochemical Oscillations and Cellular Rhythms. The Molecular Bases of Periodic and Chaotic Behaviour* (Cambridge University Press, Cambridge, 1996).
[2] A. T. Winfree, *The Geometry of Biological Time* (Springer, New York, 2001); J. D. Murray, *Mathematical Biology* (Springer, New York, 1993).
[3] A. Goldbeter, Nature (London) **420**, 238 (2002).
[4] J. Hounsgaard, H. Hultborn, B. Jespersen, and O. Kiehn, J. Physiol. (London) **405**, 345 (1988).
[5] O. Decroly and A. Goldbeter, Proc. Natl. Acad. Sci. U.S.A. **79**, 6917 (1982).
[6] M. Morita, K. Iwamoto, and M. Seno, Phys. Rev. A **40**, 6592 (1989).
[7] J. C. Leloup and A. Goldbeter, J. Theor. Biol. **198**, 445 (1999).
[8] M. Stich, M. Ipsen, and A. S. Mikhailov, Physica D **171**, 19 (2002); Phys. Rev. Lett. **86**, 4406 (2001).
[9] K. Tsumoto, T. Yoshinaga, H. Iida, H. Kawakami, and K. Aihara, J. Theor. Biol. **239**, 101 (2006).
[10] I. M. De la Fuente, BioSystems **50**, 83 (1999).
[11] F. Kaiser, Z. Naturforsch. A **33**, 294 (1978).
[12] H. Fröhlich, in *The Fluctuating Enzyme*, edited by G. R. Welch (Wiley, New York, 1986), p. 421.
[13] H. G. Enjieu Kadji, J. B. Chabi Orou, R. Yamapi, and P. Woafo, Chaos, Solitons Fractals **32**, 862 (2007).
[14] H. G. Enjieu Kadji, R. Yamapi, and J. B. Chabi Orou, Chaos **17**, 033113 (2007).
[15] R. Yamapi, H. G. Enjieu Kadji, and G. Filatrella, eprint arXiv:1001.3240v1.
[16] F. Kaiser and C. Eichwald, Int. J. Bifurcation Chaos Appl. Sci. Eng. **1**, 485 (1991).
[17] C. Eichwald and F. Kaiser, Int. J. Bifurcation Chaos Appl. Sci. Eng. **1**, 711 (1991).
[18] R. L. Kautz, Phys. Lett. A **125**, 315 (1987); J. Appl. Phys. **62**, 198 (1987); Phys. Rev. A **38**, 2066 (1988).
[19] M. I. Dykman and M. A. Krivoglaz, Sov. Phys. JETP **50**, 30 (1978).
[20] M. I. Dykman, B. Golding, L. I. McCann, V. N. Smelyanskiy, D. G. Luchinsky, R. Mannella, and P. V. E. McClintock, Chaos **11**, 587 (2001).
[21] S. Kar and D. S. Ray, Europhys. Lett. **67**, 137 (2004).
[22] C. Stambaugh and H. B. Chan, Phys. Rev. B **73**, 172302 (2006).
[23] C. Stambaugh and H. B. Chan, Phys. Rev. Lett. **97**, 110602 (2006).
[24] R. Almog, S. Zaitsev, O. Shtempluck, and E. Buks, Appl. Phys. Lett. **90**, 013508 (2007).
[25] D. G. Luchinsky, S. Beri, R. Mannella, P. V. E. McClintock, and I. A. Khovanov, Int. J. Bifurcation Chaos Appl. Sci. Eng. **12**, 583 (2002).
[26] S. Kraut and C. Grebogi, Phys. Rev. Lett. **92**, 234101 (2004).
[27] G. Filatrella, B. A. Malomed, and S. Pagano, Phys. Rev. E **65**, 051116 (2002).
[28] R. Graham, in *Stochastic Nonlinear Systems*, edited by L. Arnold and R. Lefever (Springer, New York, 1981).
[29] M. I. Freidlin and A. D. Wentzell, *Random Perturbations of Dynamical Systems* (Springer, New York, 1984).
[30] R. Graham and T. Tél, Phys. Rev. A **31**, 1109 (1985).
[31] D. E. Knuth, *The Art of Computer Programming* (Addison-Wesley, Reading, 1969), Vol. 2.
[32] R. Yamapi, B. R. Nana Nbendjo, and H. G. Enjieu Kadji, Int. J. Bifurcation Chaos Appl. Sci. Eng. **17**, 1343 (2007).
[33] H. G. Enjieu Kadji, "Synchronization dynamics of nonlinear self-sustained oscillations with applications in physics, engineering and biology," Ph.D. thesis, Université d'Abomey-Calavi, Benin, 2006.
[34] F. Kaiser, Radio Sci. **17**, 17S (1982).
[35] V.-X. Li and A. Goldbeter, J. Theor. Biol. **138**, 149 (1989).
[36] F. Kaiser, *Coherent Excitations in Biological Systems: Specific Effects in Externally Driven Self-Sustained Oscillating Biophysical Systems* (Springer-Verlag, Berlin, 1983).
[37] F. Kaiser, in *Biological Effects and Dosimetry of Nonionizing Radiation*,

edited by M. Grandolfo, S. M. Michaelson, and A. Rindi (Plenum, New York, 1983), p. 251.
[38]F. Kaiser, in *Energy Transfer Dynamics*, edited by T. W. Barret and H. A. Pohl (Springer, New York, 1987), p. 224.
[39]F. Kaiser, Kleinheubacher Berichte **32**, 395 (1989).
[40]D. Middleton, *An Introduction to Statistical Communication Theory* (McGraw-Hill, New York, 1960), Chap. 1.
[41]R. Mannella, Phys. Lett. A **254**, 3381 (1989); Int. J. Mod. Phys. C **13**, 1177 (2002).
[42]H. A. Kramers, Physica (Amsterdam) **7**, 284 (1940).
[43]V. S. Anishchenko, V. Astakhov, A. Neiman, T. Vadivasova, and L. Schimansky-Geier, *Nonlinear Dynamics of Chaotic and Stochastic Systems: Tutorial and Modern Developments* (Springer, New York, 2007).